Glass transition and dynamic-mobility spectrum of an isotropic system of rodlike molecules

Iwao Teraoka and Frank E. Karasz
Polymer Science and Engineering Department, University of Massachusetts, Amherst, Massachusetts 01003
(Received 14 October 1992)

A self-consistent mean-field theory of the glass transition is presented for the model of a high-density isotropic melt of rodlike molecules, which was originally proposed by Edwards and Evans [J. Chem. Soc. Faraday Trans. 2 **78**, 113 (1982)]. In this model, translation along the rod axis is the only mode available, but the diffusional motion of a given rod (hereafter called the test rod) is hindered by end-on collisions with the lateral surfaces of other rods that lie in its diffusion path. The basis of this treatment is the mean-field Green-function theory developed in our previous contribution for one-dimensional diffusion in the presence of many reflecting barriers [Phys. Rev. A **45**, 5426 (1992)]. A self-consistency requirement for the dynamics of the test rod and of the barrier rods leads to an asymptotic decrease to zero in the long-time diffusion constant, i.e., a glass transition, as the density of the barrier rods exceeds a critical value. The glass transition is manifested in a divergence of the lifetime τ of the barrier in a power-law $(T-T_1)^{-2}$ relation as the temperature T approaches a glass-transition temperature T_1 from above if a linear thermal contraction is assumed in the mobile phase. At a higher temperature, τ follows Arrhenius behavior. A relaxation is observed in the dynamic-mobility spectrum of rod translation with a change in the profile between the mobile and the glassy phases. We also investigate the complex modulus of the melt and find a spectral distribution similar to that for the shear modulus obtained by reptation theory for entangled linear-chain polymers.

PACS number(s): 64.70.Pf, 05.40.+j, 62.15.+i

I. INTRODUCTION

The glass transition is a phenomenon observed in a wide variety of materials [1–4]. Vast quantities of resources have been devoted to elucidating the underlying basis of this phenomenon. Researchers have extensively investigated molecular dynamics in a temperature range around the glass-transition temperature, and it is now widely accepted that the glass transition itself (when approached from above) represents a cessation of the motion of molecules or parts of molecules that are mobile above the glass-transition temperature. This behavior distinguishes the glass transition from other phase-transition phenomena in thermodynamics.

Amorphous materials composed of molecules of different sizes and molecular architectures exhibit the glass-transition phenomenon. Traditionally, this phenomenon has been explained by some variations of the free-volume theory [5–7]. In an isotropic melt of rodlike molecules (one of the materials that exhibit the glass-transition [8]) rotational and transverse motions (i.e., motions normal to the rod axis) are inhibited because of side-to-side collisions with other rodlike molecules. Only translational motion along the rod axis remains unrestricted, although the rod's diffusion constant is much reduced from that of an isolated rodlike molecule in dilute solution. Edwards and Evans [8] presented a model to explain the glass transition of an isotropic melt of rodlike molecules. The model was later refined by Edwards and Vilgis [9]. In their model, the translational motion of a rodlike molecule (hereafter called a test rod) is impeded by collisions of its ends against the sides of other rodlike molecules that lie across the diffusion path of the test rod. Even in the absence of the end collisions, the test rod is always in side-to-side contact with many other rods, and the resultant friction makes the translational motion diffusional. In the melt state, the obstructing rods (hereafter called barrier rods) diffuse along their axes away from the diffusion path of the test rod, thus enabling the test rod to move further. Translational motions of a barrier rod along its axis do not alter its hindering position along the diffusional path of the test rod until the barrier rod diffuses away. In other words, the motion of the barrier rod is irrelevant to that of the test rod until the former is no longer an obstruction. Thus, the diffusion of the test rod can be modeled as a one-dimensional Brownian particle on a random path modified by numerous "gates" that open and close stochastically. When one of the gates that has confined the particle opens, the latter is able to move into new territory. At the same rate, a new gate appears next to the particle, thereby changing the territory accessible to the particle. Repetition of this process causes the motion of the test particle to be solely diffusional. However, the diffusion constant is smaller than that in the absence of barriers.

In our previous contribution [10], we presented a mean-field Green-function (MFG) formulation to treat the dynamics of a one-dimensional Brownian particle in the presence of many random reflecting barriers that possess the same stochastic properties. The formulation allowed us to evaluate the multiple perturbation effects exerted by the barriers on the dynamics of the particle. Starting from the unperturbed Green function, i.e., a Green function for free diffusion, the average effect of the perturbation element by a single barrier is incorporated

sequentially into the perturbed Green function, resulting in a first-cumulant MFG. A functional relation between the unperturbed Green function and the first-order perturbation facilitates calculation of the first-cumulant MFG. In the next step, covariances of the perturbation elements were incorporated sequentially into the second-cumulant MFG, which can be calculated from a functional relation between the first-cumulant MFG and the second-order perturbation. Repeating this process of taking into account the higher-order correlations among the perturbation elements, we can improve the approximation to the Green function perturbed by many elements.

In an application of this scheme, we treated [10] the dynamics of a Brownian particle in the presence of fixed random reflecting barriers and of random reflecting barriers that appear on the diffusion path of the particle and later disappear. The dynamical properties in the long-wavelength limit were represented by the displacement function $q(t)$ defined as $q(t)\equiv\frac{1}{2}\langle\Delta x^2(t)\rangle$, where $\Delta x(t)$ is the displacement of the particle at time t and $\langle\ \rangle$ denotes a statistical average with respect to the original and the final (at time t) positions of the particle and to the parameters that describe the randomness of the barriers. In this treatment, we calculated $q(t)$ for the first- and second-cumulant MFG's.

In the present contribution, we treat the glass transition and the dynamics of the isotropic system of rodlike molecules at high density. The system can be a melt of such rods or a concentrated solution of rigid-chain molecules that is not in a liquid-crystalline phase. Rotational and lateral motions are prohibited, and the end collisions dominate the dynamics of translational motion along the axis, the only available mode in this system. We can apply the results for $q(t)$ obtained in the previous contribution [10] to the translational motion of the test rod in the melt, because the motion is equivalent to a one-dimensional particle diffusion in the presence of reflecting gates. Note that the rates of opening and of closing the "gates" (which are the same, so the number of the gates remains constant) are governed by the translational diffusivity of the barrier rods. Because the barrier rods and the test rod must follow common dynamics as represented by $q(t)$, a self-consistent treatment is necessary. The mean-field argument for the dynamics of both rods eliminates the difficulty associated with their correlated motions, if any. In the next section we treat the glass transition as an asymptotic decrease to zero in the long-time diffusion constant based on the self-consistent mean-field argument. Our model may appear to be similar to standard free-volume models, but the motional unit here is a rodlike molecule rather than a group of segments of variable size. In subsequent sections we consider separately the dynamics of the rods in the glassy and in the mobile phases. A primary relaxation responsible for the macroscopic diffusion of a molecule and a secondary relaxation due to localized motion are found to originate from the same mechanism. Unlike the primary relaxation, the secondary relaxation is observed in both phases.

There are difficulties in realizing an actual system that satisfies the qualifications described above for the model because of the tendency of such molecules to form nematic phases (see Edwards and Evans [8] for rationalization). However, an advantage of studying an isotropic melt of rodlike molecules is its simplicity. This system has a small number of degrees of freedom, and at high density, only the translational motion is allowed, as is assumed in this contribution. Nevertheless, it retains the properties of glass-forming liquids: each molecule interacts with many other molecules in the vicinity. We expect that the result will have features in common with those of a wide variety of amorphous materials, as mentioned by Edwards and Vilgis [9]. Another noteworthy feature of our system is that the mechanism of rod translation mimics the constraint-release mode [11,12] of entangled linear flexible chains. As we calculate the complex modulus of the isotropic melt of rodlike molecules, we will see that a spectrum similar to that of the complex shear modulus of a melt of linear flexible chains is obtained.

II. GLASS TRANSITION IN A MELT OF RODLIKE MOLECULES

Let us consider an isotropic melt of rodlike molecules of length L and diameter d, with $L>d$. We follow the end-collision model of rodlike molecules presented by Edwards and Evans [8] and denote by D_0 the translational diffusion constant of the rod along its axis in the absence of the end collisions. This mode of motion (in the absence of end collisions) is diffusional because the rod has side-to-side contact with many other rods. The diffusion constant D_0 is assumed to follow the Arrhenius law.

Let n be the average number of barriers per unit length of the diffusion path of the test rod and τ be the average lifetime of the barrier. The number of rods $c_{\rm rod}$ per unit volume of the melt is related to n by $n=\lambda L d c_{\rm rod}$, where λ is a numerical coefficient that is expected to be $\lambda\cong\pi/2$ [13].

We assume that there is no correlation between the different barrier rods that serve as obstacles to the translational diffusion of the test rod. Because the barrier rods are separated at least by a distance on the order of L, their locations and appearance and disappearance times on the diffusion path of the test rod can be considered to be uncorrelated with those of other barrier rods. Then it is possible to directly apply the results of the displacement function $q_K(t)$ obtained from the Kth cumulant MFG ($K=1,2,\dots$). In this mean-field theory, higher-order correlations between the motion of the test rod and that of the barrier rod are taken into account, and the Green function is refined, as K increases.

The Kth cumulant mean-field Green function gives the displacement function $q_K(t)$ as [10]

$$q_K(t)=\frac{q_{K-1}(t)}{[1+c_K'\xi_K(t)n^K(q_{K-1}(t)\tau/t)^{K/2}]^{2/K}} \qquad (K=1,2,\dots)\ , \quad (2.1)$$

where c_K' is a constant, and τ is the average lifetime of the barrier. The function $\xi_K(t)$ is a monotonically increasing function of t and is defined for $t\geq 0$. It expresses the de-

gree of hindrance by the barrier as time progresses and has limiting values 0 and 1 at $t=0$ and $t\to\infty$, respectively. At the average lifetime, $\xi_K(\tau)\sim 0.5$. The functional form of $\xi_K(t)$ as well as the values of c'_K depend on the probability distribution of the barrier lifetime.

The initial term of the sequence $\{q_K(t)\}$ is $q_0(t)=D_0t$. When $t\ll\tau$, the perturbation effect is not yet seen, i.e., $\xi_K(t)\cong 0$, so $q_K(t)=D_0t$. When $t\gg\tau$, $\xi_K(t)\cong 1$, and $q_K(t)$ is again proportional to t, yielding a well-defined long-time diffusion constant $D_K=\lim_{t\to\infty}[q_K(t)/t]$. When we truncate the recurrence formula at the Jth stage (J is a positive integer), we have a set of equations for $K=1,2,\ldots,J$ and expect that $q_J(t)$ is the best estimate for $q_\infty(t)$ that incorporates multiple perturbation effects to infinite order.

It was shown in our previous contribution [10] that $q_K(t)\cong D_Kt$ in the time scale longer than τ. Then, the barrier lifetime s is approximately distributed with an exponential density function $\rho(s)=\tau^{-1}\exp(-s/\tau)$, as shown in Appendix A. This density function gives $c'_1=1$, $c'_2=3-2\ln 2$, and so on.

Translational motion of the test rod follows Eq. (2.1). Self-consistency requires that it also describe the dynamics of the barrier rods along their respective axes. The barrier rod leaves the diffusion path of the test rod when it moves a distance of the order of L, i.e., $q_J(\tau)=\gamma_JL^2$, where γ_J is a numerical coefficient on the order of unity. When we set $q_K(\tau)=\gamma_KL^2$, the sequence $\{\gamma_K\}$ satisfies, from Eq. (2.1), the following recurrence formula:

$$(\gamma_K)^{-K/2}=(\gamma_{K-1})^{-K/2}+a_K(nL)^K\quad(K=1,2,\ldots,J)\ , \tag{2.2}$$

where a_K is a numerical coefficient defined by $a_K=c'_K\xi_K(\tau)$ that can be calculated; e.g., $a_1\cong 0.629$ [$\xi_1(\tau)\cong 0.629$] and $a_2\simeq 0.400$ [$\xi_2(\tau)\cong 0.248$]. The initial term is the reduced lifetime $\gamma_0=D_0\tau/L^2$ and can be regarded as a (reduced) characteristic time of the system. The sequence $\{\gamma_K\}$ ($K=1,2,\ldots$) converges to $\gamma_K\to\frac{1}{6}$ as $K\to\infty$ (see Appendix A).

When the recurrence formula is truncated at the Jth stage, γ_J is expected to be the best estimate for γ_∞, and hence we set $\gamma_J=\frac{1}{6}$. By solving the simultaneous equations given by Eq. (2.2) for $K=1,2,\ldots,J$, we obtain an expression for γ_0 as a function of nL with parameters $a_1,a_2,\ldots,a_J$. This expression is the best estimate for the reduced lifetime γ_0 when the cumulants up to order J are taken into account.

For the system to be in a mobile phase, the lifetime of the barrier must be positive and finite. Existence of a positive γ_0 leads to the condition that the number of barriers be smaller than a critical barrier density n_c, i.e., $n<n_c$, where n_c is given by

$$b_J(n_cL)^2=6\ . \tag{2.3}$$

Here $\{b_J\}$ is a sequence given by $(b_K)^{K/2}=(b_{K-1})^{K/2}+a_K$ ($K=1,2,\ldots,J$) with $b_0=0$. The long-time diffusion constant D_J in the Jth cumulant MFG is then calculated similarly by using another recurrence formula derived from Eq. (2.1):

$$D_K/D_{K-1}=[1+c'_K(nL)^K(\gamma_0D_{K-1}/D_0)^{K/2}]^{-2/K}\quad(K=1,2,\ldots,J)\ . \tag{2.4}$$

When $n>n_c$, γ_0 is infinite, and hence $D_J=0$, which means that the system then is in a glassy phase.

In the mobile phase ($n<n_c$), τ and D_J drastically change as n approaches n_c. We examine τ and D_J in two asymptotic ranges of reduced barrier density nL: (i) $nL\ll 1$ and (ii) $nL\lesssim n_cL$.

A. Asymptote for $nL\ll 1$: The liquid state

When $nL\ll 1$ and terms of order higher than $(nL)^2$ are negligible, we can terminate the recurrence formula (2.2) at the first iteration ($J=1$). Then, $\gamma_K=\gamma_1=\frac{1}{6}$ for $K\geq 2$. γ_0 is solved up to the order of nL, yielding

$$\tau=\frac{1}{6}\left[1+\frac{2}{\sqrt{6}}a_1(nL)\right]\frac{L^2}{D_0}\ , \tag{2.5}$$

which approaches the free diffusion lifetime of the barrier as nL becomes smaller. Note that this limiting value is not zero. The diffusion constant in the first-cumulant MFG is given as

$$D_1/D_0=\left[1+\frac{1}{\sqrt{6}}nL\right]^{-2}\cong\exp\left[-\frac{2}{\sqrt{6}}nL\right]\ , \tag{2.6}$$

because $nL\ll 1$.

B. Asymptote to the critical point: The glass transition

Let us truncate the recurrence formula at the second-cumulant MFG. Then, the critical density n_c is given by

$$n_cL=(6/b_2)^{1/2}=[6/(a_1^2+a_2)]^{1/2}\cong 2.75\ . \tag{2.7}$$

If we let $n=n_c-\Delta n$, τ can be obtained up to the leading order of $(\Delta n)^{-1}$, as

$$\tau=\frac{1}{(a_1+a_2/a_1)^2}\frac{L^2}{D_0}\frac{1}{(L\Delta n)^2}\cong 0.626\frac{L^2}{D_0}\frac{1}{(L\Delta n)^2}\ . \tag{2.8}$$

The diffusion constant is then given by

$$\frac{D_2}{D_0}=\frac{(a_1+a_2/a_1)^2}{c'^2_1+c'_2}\left[\frac{\Delta n}{n_c}\right]^2\cong 0.612\left[\frac{\Delta n}{n_c}\right]^2\ . \tag{2.9}$$

We can improve the approximation by taking into account higher-order cumulants, but τ and D_J have the same power dependence on Δn as in Eqs. (2.8) and (2.9). As $n\to n_c$ in the mobile phase, the lifetime τ diverges as $(\Delta n)^{-2}$, and D_2 decreases as $(\Delta n)^2$, leading eventually to the cessation of motion in the glassy phase.

If we further assume a linear thermal expansion for the mobile phase near the transition, then $\Delta n\propto T-T_1$, where T_1 is a glass-transition temperature. The lifetime τ then diverges as $D_0\tau/L^2\propto(T-T_1)^{-2}$. The diffusion constant reduces to zero as $D/D_0\propto(T-T_1)^2$, and therefore the viscosity diverges as $(T-T_1)^{-2}$. The features

we have found here for the glass transition of isotropic melt of rodlike molecules are shared by many amorphous materials; they are known to exhibit a power dependence of viscosity with an exponent of -2 in the temperature range above T_1 [14]. As T approaches T_1, however, the diffusion constant decreases, which makes it difficult to observe this power dependence in a real amorphous system.

Having examined the behavior of τ and D_J in the two limiting ranges of nL, we can now turn our attention to the intermediate range. In the second-cumulant MFG, expressions for the reduced lifetime $\gamma_0 = D_0\tau/L^2$ and the normalized diffusion constant D_2/D_0 are given, respectively, as

$$\gamma_0 = \{[6 - a_2(nL)^2]^{1/2} - a_1(nL)\}^{-2} \tag{2.10}$$

and

$$D_2/D_0 = \{[1 + c_1'\gamma_0^{1/2}(nL)]^2 + c_2'\gamma_0(nL)^2\}^{-1} . \tag{2.11}$$

In Fig. 1 are plotted the reciprocal of the reduced lifetime, $1/\gamma_0$, and the normalized diffusion constant, D_2/D_0, for the whole range of $nL < n_cL \cong 2.75$. Note that nL is a linear function of $1/T$ if linear thermal expansion is assumed for the mobile phase. In the limit of $nL \to 0$, $1/\gamma_0 \to 6$ and $D_2/D_0 \to 1$. Except in the near-transition range, the curves for τ and D_2 can be fitted by Williams-Landel-Ferry (WLF) equations [15], if we consider the dependence of D_0 on the temperature to follow the Arrhenius law.

In the second-cumulant MFG, $c_{\text{rod},c} \cong 1.75/dL^2$ at the glass transition. The volume fraction of rods is $\phi_{\text{rod},c} \cong 1.38(d/L)$. Although there is an ambiguity in the estimation of the numerical coefficient for $\phi_{\text{rod},c}$, its dependence on d/L implies that the transition will occur at a low volume fraction of rods.

In this contribution, we assumed that translational diffusion of a barrier rod was the sole mechanism for removing it from the diffusion path of the test rod. Even at high concentration, there is a nonzero local diffusivity in rotation and lateral translation, which can constitute other paths leading to the disappearance of a barrier. Note, however, that both the rotational and the translational diffusion constants at high concentration (isotropic) depend on the translational diffusivity along the axis [16,17]. Thus we should be able to construct a self-consistency argument similar to the one developed in this section and should arrive at a similar result for the glass transition, as long as the system is in an isotropic phase. The second mechanism for the barrier disappearance will decrease the lifetime of the barrier, and therefore n_cL in Eq. (2.3) and $\phi_{\text{rod},c}$ will become larger.

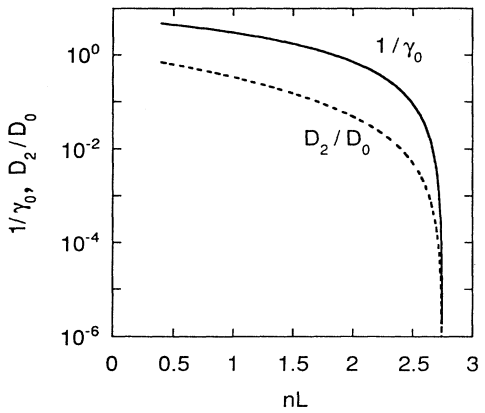

FIG. 1. Plots of the reciprocal of reduced lifetime $1/\gamma_0 = L^2/D_0\tau$ (solid line) and of the normalized diffusion constant D_2/D_0 (dashed line) calculated in the second-cumulant MFG theory for a mobile phase ($nL < n_cL \cong 2.75$). The abscissa is nL, the number of barrier rods intercepting a section (length L) of the diffusion path of the test rod.

Imposing a self-consistency condition for the dynamics of a test rod and the barrier rods, we derived glass-transition characteristics for an isotropic melt of rodlike molecules in terms of a vanishing of the long-time diffusion constant. As we have pointed out, the mechanism of restriction on the translational motion of the rod resembles the constraint-release mode claimed to exist in a melt of linear flexible chains [11,12]. The similarity might lead to a development of a theory of glass transition for the melt of linear flexible chains. Note that, unlike many other models for the glass transition, this theory can be constructed on a molecular level.

III. DYNAMIC-MOBILITY SPECTRUM IN THE GLASSY PHASE

In the glassy phase, the long-time diffusion constant is zero. However, the rods still can undergo translational motion in a domain demarcated by two barrier rods. In the short-time limit, the translational motion over a short distance reduces to the unperturbed diffusion. The dynamic behavior of the translational motion in a different time scale is well represented by the dynamic-mobility spectrum of the rods in the frequency domain, which we derive in this section.

A time-dependent mobility $\mu(t)$, normalized by the unperturbed value D_0k_BT, where k_B is the Boltzmann constant and T the absolute temperature, is defined in general as

$$\mu(t) = \frac{1}{D_0}\frac{dq(t)}{dt} . \tag{3.1}$$

The Fourier transformation of its time derivative is a dynamic mobility μ^* at an angular frequency ω:

$$\begin{aligned}\mu^* &= \mu(0) + \int_0^\infty e^{-j\omega t}\frac{d\mu(t)}{dt}dt \\ &= j\omega\int_0^\infty e^{-j\omega t}\mu(t)dt \\ &= (j\omega)^2\int_0^\infty e^{-j\omega t}\frac{q(t)}{D_0}dt ,\end{aligned} \tag{3.2}$$

where j is an imaginary unit. The bulk mobility tensor has nonzero diagonal elements $\mu_{xx} = \mu_{yy} = \mu_{zz} = \mu^*/3$. The mean-field argument eliminates off-diagonal elements.

In the glassy state, the translation along the rod axis is constrained by the barriers intercepting the path of

translational motion of the rod. The dynamics are equivalent to those of a particle confined in a fixed well. Its width W is distributed with probability density function $n^2W\exp(-nW)$, where n is the average number density of the barriers [18]. The dynamic mobility μ^* in one dimension is calculated as

$$\mu_G^*=1+2(j\nu)^{-1/2}-\frac{4}{j\nu}\beta((j\nu)^{-1/2}) , \tag{3.3}$$

where $\nu\equiv\omega/(n^2D_0)$ is a reduced frequency [see Appendix B for derivation of Eq. (3.3) and the definition of the beta function $\beta(x)$] and the subscript G denotes the glassy state. Its low- and high-frequency limits are 0 and 1, respectively. The low- and high-frequency asymptotes are given, respectively, by

$$\mu_G^*=\tfrac{1}{2}(j\nu)-(j\nu)^2+\cdots \tag{3.4}$$

and

$$\begin{aligned}\mu_G^*&=1-2(j\nu)^{-1/2}+4\ln 2(j\nu)^{-1}-\tfrac{2}{3}\pi^2(j\nu)^{-2}+\cdots\\&=[1+2(j\nu)^{-1/2}+4(1-\ln 2)(j\nu)^{-1}\\&\quad+8(1-2\ln 2)(j\nu)^{-3/2}+\cdots]^{-1} .\end{aligned} \tag{3.5}$$

To evaluate the first- and second-cumulant MFG approximations, we calculate the dynamic mobility for each case. If we employ the result of the first-cumulant MFG applied to the dynamics of a particle in a system with fixed random barriers [10], the mobility is given by

$$\mu_{G1}(t)=[1+c_1n(D_0t)^{1/2}]^{-3} , \tag{3.6}$$

where $c_1=4/(3\pi^{1/2})$. Its counterpart in the frequency domain is

$$\mu_{G1}^*=(j\nu')^2\int_0^\infty e^{-j\nu'u}\frac{u}{(1+\sqrt{u})^2}du , \tag{3.7}$$

with $u=c_1^2n^2D_0t$ and $\nu'=\nu/c_1^2=(9\pi/16)\nu$. The integral leads to the result

$$\begin{aligned}\mu_{G1}^*&=j\nu'-2\sqrt{\pi}(j\nu')^{3/2}-2(j\nu')^2+2\sqrt{\pi}(j\nu')^{5/2}\\&\quad+(j\nu')^2(2j\nu'-3)e^{-j\nu'}\\&\quad\times[\mathrm{Ei}(j\nu')+j2\sqrt{\pi}\,\mathrm{erfc}(e^{-j\pi/4}\sqrt{\nu'})] ,\end{aligned} \tag{3.8}$$

where $\mathrm{Ei}(jy)\equiv-\int_y^\infty[\exp(jt)/t]dt$ for $y>0$, and $\mathrm{erfc}(z)$ for a complex argument is an analytical continuation of the error function defined as $\mathrm{erfc}(x)\equiv\int_x^\infty\exp(-t^2)dt$ for $x>0$. In the low-frequency limit, Eq. (3.8) becomes asymptotically

$$\mu_{G1}^*=\frac{9\pi}{16}j\nu-\frac{27\pi^2}{32}(j\nu)^{3/2}+\cdots . \tag{3.9}$$

In the high-frequency limit,

$$\mu_{G1}^*=\left[1+2(j\nu)^{-1/2}+4\left[1-\frac{8}{3\pi}\right](j\nu)^{-1}+8\left[1-\frac{28}{9\pi}\right](j\nu)^{-3/2}+\cdots\right]^{-1} . \tag{3.10}$$

Application of the second-cumulant MFG theory yields the following time-dependent mobility [10]:

$$\mu_{G2}(t)=\frac{1+c_1n(D_0t)^{1/2}}{[1+2c_1n(D_0t)^{1/2}+(c_1^2+c_2)n^2D_0t]^2} \tag{3.11}$$

with $c_2\equiv-2\ln 2+3c_1^2\cong 0.311\,36$. The complex mobility is then given by

$$\mu_{G2}^*=(j\nu')^2\int_0^\infty\exp(-j\nu'u)\frac{u}{1+2\sqrt{u}+(1+c_2/c_1^2)u}du . \tag{3.12}$$

The frequency spectrum of μ_{G2}^* was calculated numerically. The asymptotes in the low and high frequencies are, respectively,

$$\mu_{G2}^*=\left[\frac{64}{9\pi}-2\ln 2\right]^{-1}(j\nu)-\frac{8}{3}\left[\frac{64}{9\pi}-2\ln 2\right]^{-2}(j\nu)^{3/2}+\cdots \tag{3.13}$$

and

$$\mu_{G2}^*=\left[1+2(j\nu)^{-1/2}+4(1-\ln 2)(j\nu)^{-1}+4\left[2+\ln 2-\frac{80}{9\pi}\right](j\nu)^{-3/2}+\cdots\right]^{-1} . \tag{3.14}$$

Figure 2 shows the real and imaginary parts of the dynamic-mobility spectrum $\mu_G^*=\mu_G'+j\mu_G''$ (solid line) and its approximations by the first- and the second-cumulant MFG theories, $\mu_{G1}^*=\mu_{G1}'+j\mu_{G1}''$ (dashed line) and $\mu_{G2}^*=\mu_{G2}'+j\mu_{G2}''$ (dash-dotted line), respectively, plotted against reduced frequency $\nu\equiv\omega/(n^2D_0)$. A relaxation pattern is evident. The dispersion curve is very broad, extending over several decades in the frequency domain. The first- and second-cumulant MFG theories provide a close approximation except in the low-

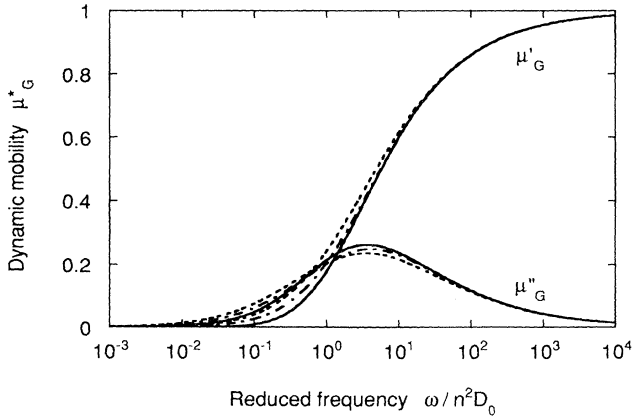

FIG. 2. Frequency spectra of the real part μ' and the imaginary part μ'' of the dynamic mobility μ^* of an isotropic system of rodlike molecules in the glassy phase. Results for the exact solution, the first-cumulant MFG, and the second-cumulant MFG are plotted as solid, dashed, and dash-dotted lines, respectively.

TABLE I. Profile of the imaginary part of the dynamic mobility. The half widths at half maximum are in units of decades of reduced frequency.

Approximation method	Peak height	Peak frequency $\nu_S=\omega_S/n^2D_0$	Half width
μ''_G	0.263	3.65	2.29
μ''_{G1}	0.236	3.54	2.57
μ''_{G2}	0.250	4.10	2.41
Debye relaxation	0.5	NA[a]	1.144

[a]NA, not applicable.

frequency range; the MFG theories emphasize the deviations in the dynamics from free diffusion ($\mu^*=1$) in the short-time scale. The second-cumulant MFG provides better agreement with μ^*_G than does the first-cumulant MFG, as expected. Peak heights, peak frequencies $\nu_S=\omega_S/(n^2D_0)$, and half widths at half maximum of the imaginary components are listed in Table I. For reference, those of a Debye-type relaxation are also listed. We curve-fitted μ^* in the complex plane to a Havriliak-Negami response function [19]:

$$\mu^*=\mu_0+\Delta\mu\{1-[1+(j\omega\tau_R)^\alpha]^{-\beta}\}\ , \tag{3.15}$$

where τ_R is a relaxation time, and the parameters α and β describe the breadth and skewness of the distribution in the Debye-type relaxation time, respectively. Nonlinear curve fitting for the calculated spectra in the frequency range $10^{-2}\le\nu\le10^4$ yields satisfactory fits. The parameters obtained are listed in Table II together with reference values for the Debye-type relaxation with a single relaxation time.

The breadth also can be represented in a Cole-Cole plot of dynamic mobility, shown in Fig. 3. Obviously, the relaxation spectrum of μ^*_G follows an inverse lemniscate, whereas μ^*_{G1} and μ^*_{G2} are closer to the Cole-Cole pattern. The curve of μ^*_G intercepts the real axis at angles $\pi/2$ (toward $\mu'=0$) and $\pi/4$ (toward $\mu'=1$) in the low- and high-frequency limits, respectively. The intercept angles of μ^*_{G1} and μ^*_{G2} at high frequency are the same as those of μ^*_G, but at low frequency these angles differ. The low-frequency asymptotes of μ^*_{G1} and μ^*_{G2} have a dominant component $-(j\nu)^{3/2}$ reflecting incompleteness of the finite-order cumulant MFG theories.

The dynamic mobility we obtained here shows diffusional characteristics at high frequencies, because we postulated free diffusion for a rod between the barriers

TABLE II. Havriliak-Negami fitting parameters for the dynamic mobility.

Approximation method	$n^2D_0\tau_R$	α	β
μ^*_G	0.560	0.769	0.535
μ^*_{G1}	0.292	0.643	0.657
μ^*_{G2}	0.259	0.686	0.632
Debye relaxation	NA[a]	1	1

[a]NA, not applicable.

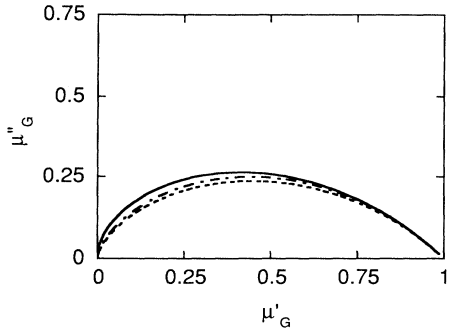

FIG. 3. Cole-Cole plots of dynamic mobility μ^* of an isotropic system of rodlike molecules in the glassy phase. Results for the exact solution, the first-cumulant MFG, and the second-cumulant MFG are plotted as solid, dashed, and dash-dotted lines, respectively.

and no other mechanism for any kind of motion. In real systems, the elastic characteristics of rodlike molecules toward bending stresses will eventually dominate at even higher frequencies, which will lead to $\mu^*\propto j\omega$.

The relaxation mode observed for μ^*_G in the glassy phase is associated with local motion. It can be designated as a secondary relaxation as opposed to the primary, glass-mobile relaxation. The secondary relaxation is widely observed in many glass materials as a relaxation mode that appears at a temperature lower than the glass-transition temperature. In the following section, we discuss this relaxation mode in conjunction with the primary relaxation related to the glass transition.

IV. DYNAMIC-MOBILITY SPECTRUM IN THE MOBILE PHASE

The mobile phase is characterized by a finite barrier lifetime and a nonzero dc mobility [$\mu^*(\omega=0)$]. In this section, we obtain the frequency profile of the dynamic-mobility spectrum of a rodlike molecule with a finite barrier lifetime. We also investigate the complex modulus m^*, which is defined in the normalized form as

$$m^*=\frac{1}{n^2D_0}\frac{j\omega}{\mu^*}=\frac{1}{\zeta^2}\frac{j\omega\tau}{\mu^*}\ , \tag{4.1}$$

where τ is the average lifetime of the barrier, and $\zeta=n(D_0\tau)^{1/2}$ is a dynamic hindrance factor that varies in the range above $nL/\sqrt{6}$. It is assumed here that the mobility of any part of the system is derived from μ^*, the translational diffusivity of the rods. In the mean-field argument for the isotropic melt of rodlike molecules, m^* defined here in one dimension is proportional to the shear modulus G^*. We investigate in this section the spectral features of μ^* and m^* as ζ is changed. Note that the barrier lifetime τ, which goes to infinity as the system approaches the glass transition, is the dominantly varying factor in ζ. It will be shown that, for all values of ζ, m^* is characterized by two relaxation times, one being associated with the lifetime of the barrier and the other with the relaxation time for the secondary relaxation.

For stochastic barriers with finite lifetimes, we do not have an exact expression for μ^*. Therefore below we em-

ploy the results of the first- and the second-cumulant MFG theories.

When the first-cumulant MFG theory is applied to particle diffusion in stochastic barriers with lifetime s distributed with density $\rho(s)=\tau^{-1}\exp(-s/\tau)$, the displacement function is given by [10]

$$q_{M1}(t)=\frac{D_0 t}{[1+\zeta\xi_1(t/\tau)]^2} . \tag{4.2}$$

The subscript M denotes the mobile phase. The hindrance function ξ_1 for the first-cumulant MFG is given by [10]

$$\xi_1(\mu)=\frac{e^{-u}}{\sqrt{\pi u}}+\left[1-\frac{1}{2u}\right]\mathrm{erf}\sqrt{u} , \tag{4.3}$$

where $\mathrm{erf}(x)\equiv\int_0^x\exp(-t^2)dt$. The dynamic mobility μ^*_{M1} in the first-cumulant MFG is then obtained as

$$\mu^*_{M1}=(j\omega\tau)^2\int_0^\infty e^{-j\omega\tau u}\frac{u}{[1+\zeta\xi_1(u)]^2}du , \tag{4.4}$$

where $u=t/\tau$.

Since the integration in Eq. (4.4) appears involved, we concentrate here on their asymptotes. The low- and high-frequency asymptotic expansions for μ^*_{M1} are, respectively,

$$\mu^*_{M1}=\frac{1}{(1+\zeta)^2}\left[1+\frac{\zeta}{1+\zeta}j\omega\tau-\frac{2\zeta}{1+\zeta}(j\omega\tau)^2+\cdots\right] \tag{4.5}$$

and

$$\mu^*_{M1}=\left[1+2\zeta(j\omega\tau)^{-1/2}+4\left[1-\frac{8}{3\pi}\right]\zeta^2(j\omega\tau)^{-1}+\cdots\right]^{-1} . \tag{4.6}$$

Equation (4.6) coincides with Eq. (3.10) obtained above for the glassy phase. The high-frequency characteristics in the mobile phase are the same as those in the glassy phase. They represent a short-time, localized motion in the presence of barriers fixed at least in the relevant time scale. They are not responsible for the macroscopic mobility of the rodlike molecules.

If we use Eq. (4.5) for μ^* in Eq. (4.1), we obtain a low-frequency asymptote for the complex modulus m^*_{M1} in the first-cumulant MFG:

$$m^*_{M1}=\frac{1}{\zeta^2}\frac{j\omega\tau}{\mu^*_{M1}}=\left[1+\frac{1}{\zeta}\right]^2\frac{j\omega\tau}{1+\frac{\zeta}{1+\zeta}j\omega\tau-\frac{2\zeta}{1+\zeta}(j\omega\tau)^2+\cdots} . \tag{4.7}$$

The loss modulus $m''_{M1}=\mathrm{Im}[m^*_{M1}]$ in the low-frequency asymptote is

$$m''_{M1}=\omega\tau(1+1/\zeta)^2\left[1-\frac{\zeta(2+3\zeta)}{(1+\zeta)^2}(\omega\tau)^2\right] . \tag{4.8}$$

When $\zeta\gg1$, a local maximum appears in m''_{M1} at a frequency ω_P given by

$$\omega_P\tau\cong\frac{1+\zeta}{\sqrt{3\zeta(2+3\zeta)}} , \tag{4.9}$$

which approaches $\frac{1}{3}$ as $\zeta\to\infty$. The relaxation time associated with this peak is close to τ, and hence this relaxation mode is a primary relaxation leading eventually to the glass transition. In a frequency range above ω_P, the storage modulus $m'_{M1}=\mathrm{Re}[m^*_{M1}]$ for $\zeta\gg1$ shows a plateau of $16/(9\pi)$. When $\omega\ll\omega_P$, $m'_{M1}=(1+1/\zeta)(\omega\tau)^2$.

The high-frequency characteristics of m^*_{M1} are obtained by using Eq. (4.6) for μ^*:

$$m^*_{M1}=\frac{j\omega}{n^2D_0}\left[1+2(j\omega/n^2D_0)^{-1/2}+4\left[1-\frac{8}{3\pi}\right](j\omega/n^2D_0)^{-1}+\cdots\right] . \tag{4.10}$$

The real and imaginary components are approximated by $m'_{M1}\cong(2\omega/n^2D_0)^{1/2}$ and $m''_{M1}\cong\omega/n^2D_0$, respectively.

Now we turn to the second-cumulant MFG theory. The dynamic mobility μ^*_{M2} is given as [10]

$$\mu^*_{M2}=(j\omega\tau)^2\int_0^\infty e^{-j\omega\tau u}\frac{u}{[1+\zeta\xi_1(u)]^2+c'_2\zeta^2\xi_2(u)}du , \tag{4.11}$$

where

$$\xi_2(u)=\frac{3}{c'_2}\xi_1(u)^2-\frac{2\ln2}{c'_2}\left[1-\frac{1}{2u}(1-e^{-2u})\right] . \tag{4.12}$$

The low- and high-frequency asymptotes are, respectively,

$$\mu^*_{M2}=\frac{1}{(1+\zeta)^2+c'_2\zeta^2}\times\left[1+\frac{\zeta+\frac{1}{2}(5+c'_2)\zeta^2}{(1+\zeta)^2+c'_2\zeta^2}j\omega\tau-\frac{\frac{1}{2}\zeta(4+(13+c'_2)\zeta)}{(1+\zeta)^2+c'_2\zeta^2}(j\omega\tau)^2+\cdots\right] \tag{4.13}$$

and

$$\mu^*_{M2}=[1+2\zeta(j\omega\tau)^{-1/2}+4(1-\ln2)\zeta^2(j\omega\tau)^{-1}+\cdots]^{-1} . \tag{4.14}$$

In analogy to the first-cumulant MFG results, Eq. (4.14) is equivalent to Eq. (3.14) obtained for the glassy phase.

The dynamic modulus m^*_{M2} in the second-cumulant MFG is obtained similarly from Eqs. (4.1) and (4.11). The overall behavior of m^*_{M2} is similar to that of m^*_{M1}: when $\zeta\gg1$, a local maximum is observed in m''_{M2} at a

frequency ω_P given by $\omega_P\tau \cong 0.275$. The plateau modulus is about 0.877. At high frequency, the behavior is the same.

We show plots for μ^*_{M2} and m^*_{M2} calculated by numerical Fourier transformation. The plots are for the second-cumulant MFG only; the results for the first-cumulant MFG are similar.

Figure 4 shows curves for $\mu'_{M2}=\mathrm{Re}[\mu^*_{M2}]$ and $\mu''_{M2}=\mathrm{Im}[\mu^*_{M2}]$, respectively, for the dynamic hindrance factor $\zeta \equiv n(D_0\tau)^{1/2}=10^1$ (solid line), 10^0 (dashed line), $10^{-1/2}$ (dash-dotted line), and 10^{-1} (dotted line), plotted against the reduced frequency ω/n^2D_0. The peak frequency $\omega_S/(n^2D_0)$ of μ''_{M2} shifts to a higher frequency, and the peak profile for μ''_{M2} becomes sharper, as ζ decreases, i.e., as the rods become more mobile. The half widths of μ''_{M2} are 2.12, 1.82, 1.75, and 1.65 decades, respectively for the four values of ζ (cf. 2.41 decades for fixed barriers in the glassy phase; see Table I). Cole-Cole plots for μ^*_{M2} are shown in Fig. 5. At high frequency, the Cole-Cole plot for smaller ζ follows that for μ^*_{M2}, but deviates from it at a frequency around ω_S and levels off to $\mu'_{M2}(\omega=0)$ in the low-frequency limit.

Figure 6 shows curves for m'_{M2} (solid line) and m''_{M2} (dashed line) plotted against ω/n^2D_0, for dynamic hindrance factors $\zeta=10^{-1}$, $10^{-1/2}$, 10^0, $10^{1/2}$, 10^1, $10^{3/2}$, and 10^2. For reference, $m^*_{G2}=j\omega/(n^2D_0\mu^*_{G2})$ calculated for fixed barriers by using Eq. (3.12) is also plotted. As predicted in the asymptotes, there is a local peak in m''_{M2} at a frequency ω_P given by $\omega_P/n^2D_0 \cong 0.275/\zeta^2$, which shifts to a lower frequency as ζ increases and the system approaches the glass transition. A plateau modulus is observed when $\zeta > 10$. This primary relaxation is of the Debye type. In the time scale longer than τ, the dynamics are diffusional with a long-time diffusion constant that varies with ζ. At high frequencies, the dynamics are again diffusional, but with the diffusion constant D_0, and therefore the curves for different values of ζ merge into a single curve expressed as $m^*_{M2} \cong j\omega/n^2D_0 + 2(j\omega/n^2D_0)^{1/2}$. This secondary relaxation in the normalized modulus remains nearly the same throughout the mobile phase and the glassy phase. Compared with the primary relaxation, the secondary relaxation is broader, as seen in Fig. 4, characteristic of a confined motion.

It is interesting to note a similarity between the modulus calculated here for an isotropic melt of rodlike molecules and the shear modulus of a melt of flexible linear-chain polymers. (See Onogi, Masuda, and Kitagawa [20] and Marin and Graessley [21] for typical experimental results, and Doi and Edwards for the reptation theory [22].) The asymptotic behaviors in the low-frequency limits of the moduli are the same, as represented in the frequency dependence of m^* ($m' \propto \omega^2$, $m'' \propto \omega$) and in the existence of a plateau modulus. Although the detailed mechanism for the overall diffusion is different between our model and that involved in the reptation

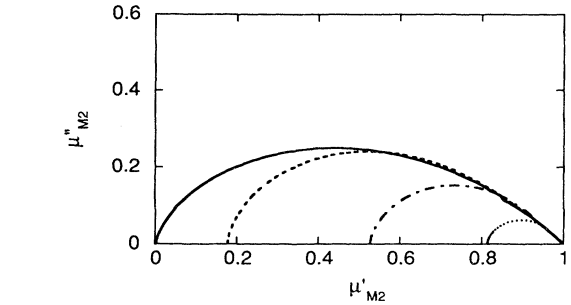

FIG. 5. Cole-Cole plots of the dynamic mobility μ^*_{M2} of an isotropic melt of rodlike molecules in the mobile phase. Results for the second-cumulant MFG are shown here. The dynamic hindrance factor $\zeta=n(D_0\tau)^{1/2}$ is 10^1 (solid line), 10^0 (dashed line), $10^{-1/2}$ (dash-dotted line), and 10^{-1} (dotted line).

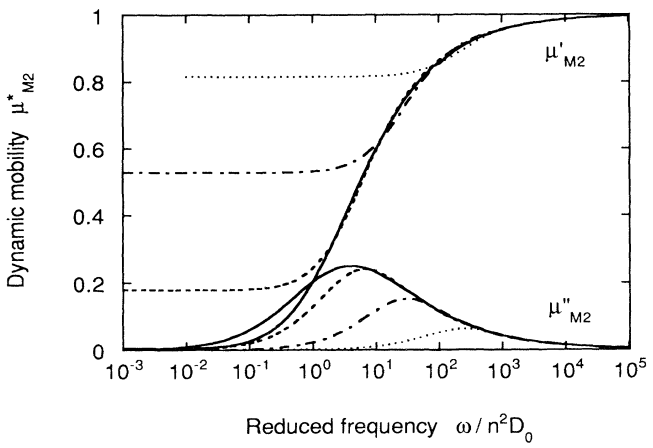

FIG. 4. Frequency spectra of the real part μ'_{M2} and the imaginary part μ''_{M2} of the dynamic mobility μ^*_{M2} of an isotropic melt of rodlike molecules in the mobile phase. Results for the second-cumulant MFG are shown here. The dynamic hindrance factor $\zeta \equiv n(D_0\tau)^{1/2}$ is 10^1 (solid line), 10^0 (dashed line), $10^{-1/2}$ (dash-dotted line), and 10^{-1} (dotted line).

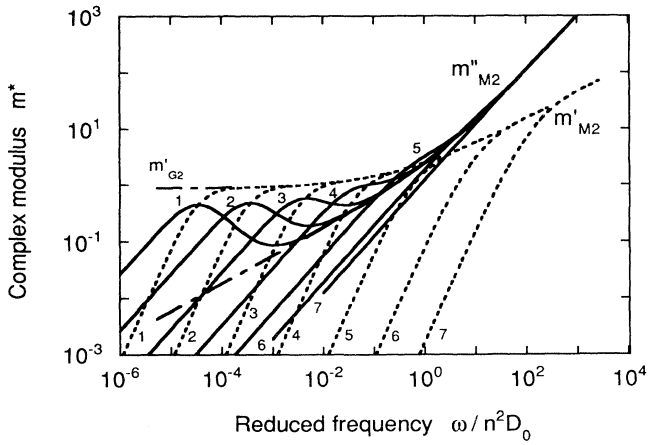

FIG. 6. Frequency spectra of the real part m'_{M2} (dashed line) and the imaginary part (solid line) m''_{M2} of the complex modulus m^*_{M2} of an isotropic melt of rodlike molecules in the mobile phase. Results for the second-cumulant MFG are shown here. The dynamic hindrance factor $\zeta=n(D_0\tau)^{1/2}$ is (1) 10^2; (2) $10^{3/2}$; (3) 10^1; (4) $10^{1/2}$; (5) 10^0; (6) $10^{-1/2}$; and (7) 10^{-1}. For reference, m^*_{G2} calculated for the glassy phase is also plotted as the dash-dotted line.

theory, the following critical feature is common: The diffusion of the center of mass is made possible when the constraint imposed by other similar molecules disappears, either by self-diffusion of the test chain or by the diffusion of the barrier rods. As the time scale of the constraint (the barrier lifetime or the disengagement time) becomes longer, the relaxation frequency shifts to a lower frequency.

The high-frequency asymptotic behavior is different, however. In the reptation theory, the high-frequency dynamics of a melt of flexible chains reduce to those of a Rouse chain [22]. The resultant complex modulus for $\omega\tau_e \gtrsim 1$ (τ_e is the time in which segmental displacement equals the tube diameter) is expressed as $G^*(\omega)/G_N=\sqrt{\pi}(j\omega\tau_e)^{1/2}$, where G_N is a plateau modulus. Our model yields $G''(\omega)\sim\omega$ because of the diffusional characteristics at high frequencies.

To estimate the relaxation frequency ω_P of the primary relaxation also in the small ζ range, we calculated a response function $j\omega\tau[(1/\mu^*)-1-2\zeta(j\omega\tau)^{-1/2}]$ and located the peak frequency in its imaginary part as ω_P. The two relaxation frequencies ω_P and ω_S reduced by n^2D_0 are plotted in Fig. 7 against the dynamic hindrance factor $\zeta=n(D_0\tau)^{1/2}$. The two relaxation modes merge as ζ becomes smaller, i.e., as the system approaches the liquid limit. As the system approaches the glass transition and ζ becomes larger, ω_P decreases as ζ^{-2} [which is proportional to $(T-T_1)^2$ when linear thermal expansion is assumed], whereas ω_S converges to the value in the glassy phase (cf. Table I). Note that D_0, a factor in the denominator, also depends on the temperature, most likely following the Arrhenius law. Then, ω_S follows the Arrhenius law in the glassy phase, a behavior that continues into the mobile phase. With further increase in the temperature, ω_S begins to deviate from the Arrhenius law. However, the deviation will be blurred by the merger of the two relaxation modes.

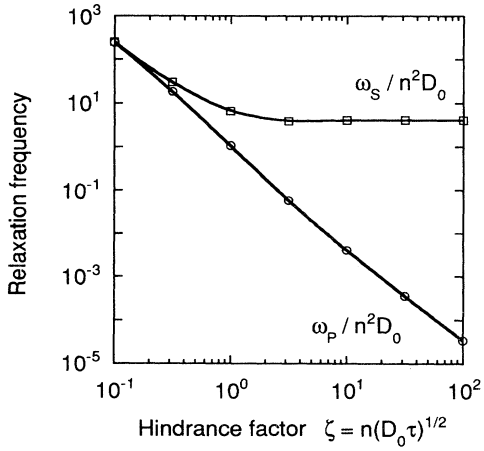

FIG. 7. Relaxation frequencies ω_P and ω_S reduced by n^2D_0 of the primary and secondary relaxations in the mobile phase are plotted against the dynamic hindrance factor $\zeta=n(D_0\tau)^{1/2}$. Symbols are the calculated values; the lines are to guide the eye.

V. CONCLUDING REMARKS

Using the model of an isotropic melt of rodlike molecules and a self-consistency argument for the dynamics of rod translation, we have described the glass-transition phenomena in terms of a loss of dc mobility. With the additional assumption of linear thermal expansion in the mobile phase, the relaxation frequency of the primary relaxation responsible for the glass transition was found to decrease in a power law $(T-T_1)^2$ as the temperature T approaches a glass-transition temperature T_1. At a higher temperature, the relaxation frequency follows WLF behavior, approaching behavior described by the Arrhenius law only at very high temperatures. A secondary relaxation as represented in the dynamic-mobility spectrum is observed throughout the glassy and mobile (liquid) phases. The latter relaxation follows an Arrhenius law and merges with the primary relaxation when the temperature is much higher than T_1. Although we have specifically investigated an isotropic system of rodlike molecules at high density, we expect that the results demonstrate common features with respect to the characteristics of the glass transition and of the two relaxation modes observed in a wide variety of materials of complex intermolecular interaction.

The similarity between the results for the complex moduli for our model and for a melt of linear flexible chains may lead to another theoretical model for the dynamics of entangled linear-chain polymers. By calculating the first-order perturbation to the normal modes of the chain dynamics and by using the first-order cumulant MFG theory or higher order, we may be able to account for the chain dynamics in melts and semidilute solutions without assuming a tube hypothesis. We also expect that we can derive results for the complex modulus in a single equation valid over a wide range of frequencies.

ACKNOWLEDGMENT

This work was supported in part by the Air Force Office of Scientific Research Grant No. 92-001.

APPENDIX A: DISTRIBUTION OF LIFETIMES

The first exit time t of a Wiener process $X(t)$ with diffusion constant D in one dimension from an interval $[0,L]$ when $X(0)=y$ $(0\le y\le L)$ has a probability distribution function $F(t;y)$ [23]:

$$F(t;y)=1-\frac{2}{\pi}\sum_{j=0}^{\infty}\frac{(-1)^j}{j+\frac{1}{2}}[\cos(j+\tfrac{1}{2})\pi(2y/L-1)]\times\exp(-\alpha_j t) \quad \text{(A1)}$$

with

$$\alpha_j=4(j+\tfrac{1}{2})^2\pi^2 D/L^2 . \quad \text{(A2)}$$

For a barrier rod problem, $X(t)$ is the translational diffusion of the rod along the axis, and y is the distance of one of its ends from the blocking point across the diffusion path of the test rod. The corresponding probability-density function (PDF) $f(t;y)$ is

$$f(t;y)=-\frac{\partial F(t;y)}{\partial t}$$
$$=8\pi\frac{D}{L^2}\sum_{j=0}^{\infty}(-1)^j(j+\tfrac{1}{2})\times\cos[(j+\tfrac{1}{2})\pi(2y/L-1)]\times\exp(-\alpha_j t)\ . \quad \text{(A3)}$$

The lifetime of the barrier is equal to the time between the last entry into and the first exit from $[0,L]$ of a Wiener process $X(t)$. Let us choose a time when $X(t)=y$ is in $[0,L]$. The first exit time t_1 since then has a PDF $f(t_1;y)$. The last entry time $t-t_1$, the time that has elapsed since the last entry into $[0,L]$, has a PDF $f(t-t_1;y)$, because the last entry is a time-reversal event to the first exit. The PDF for the lifetime t is then given by a convolution:

$$f_C(t;y)=\int_0^t f(t_1;y)f(t-t_1;y)dt_1\ . \quad \text{(A4)}$$

Averaging with respect to y yields

$$f_C(t)=L^{-1}\int_0^L f_C(t;y)dy$$
$$=\tfrac{1}{2}(8\pi D/L^2)^2\sum_{j=0}^{\infty}(j+\tfrac{1}{2})^2 t\exp(-\alpha_j t)\ . \quad \text{(A5)}$$

The average lifetime τ is then given as

$$\tau=\int_0^\infty t f_C(t)dt=\tfrac{1}{6}L^2/D\ . \quad \text{(A6)}$$

Numerical calculation of the probability distribution function corresponding to $f_C(t)$ shows that it is well approximated by $1-\exp(-t/\tau)$.

A closer examination of Fig. 4 in our previous contribution [10] reveals that the particle motion in the presence of stochastic random barriers is nearly diffusional in the time scale longer than the lifetime of the barrier τ, but with a diffusion constant much reduced from the unperturbed value. Note that plots in the figure were calculated assuming an exponential distribution for the lifetimes.

The mean-square displacement of the barrier rod in time τ is $2D\tau=\frac{1}{3}L^2$. The barrier disappears by returning to an end point that is the same as the entry point or by going to the other one. This value for the mean-square displacement is the same also for other stochastic processes represented by a transition probability $P(x,x';t)$ from position x' at time 0 to position x at time t:

$$P(x,x';t)=\frac{1}{\sqrt{4\pi q(t)}}\exp\left[-\frac{(x-x')^2}{4q(t)}\right] \quad \text{(A7)}$$

with monotonically increasing $q(t)$.

APPENDIX B: MOBILITY OF A BROWNIAN PARTICLE IN A WELL

A Green function $G(x,x';t;W)$ for a one-dimensional Brownian particle in a well $[0,W]$ with reflecting boundaries at both ends is explicitly given as

$$G(x,x';t;W)=\frac{1}{W}+\frac{2}{W}\sum_{l=1}^{\infty}\cos\frac{l\pi x}{W}\cos\frac{l\pi x'}{W}\times\exp[-(l\pi/W)^2D_0t]\ , \quad \text{(B1)}$$

where D_0 is the unperturbed diffusion constant. The displacement function $q(t;W)\equiv\langle(x-x')^2\rangle/2$ is then calculated as

$$q(t;W)=\frac{8}{\pi^4}W^2\sum_{\substack{l=1\\(l\ \text{odd})}}^{\infty}\frac{1}{l^4}\{1-\exp[-(l\pi/W)^2D_0t]\}\ , \quad \text{(B2)}$$

where the odd integer l takes on values from 1 to infinity. Equation (B2) yields the mobility $\mu(t)$ from Eq. (3.1) as

$$\mu(t;W)=\frac{8}{\pi^2}\sum_{\substack{l=1\\(l\ \text{odd})}}^{\infty}\frac{1}{l^2}\exp[-(l\pi/W)^2D_0t]\ . \quad \text{(B3)}$$

The dynamic mobility is then obtained as

$$\mu^*(\omega;W)=\frac{8}{\pi^2}\sum_{\substack{l=1\\(l\ \text{odd})}}^{\infty}\frac{j\omega}{j\omega+(l\pi/W)^2D_0}\frac{1}{l^2}$$
$$=1-rW\tanh(rW) \quad \text{(B4)}$$

with $r\equiv\frac{1}{2}(j\omega/D_0)^{1/2}$. Now we take an average of $\mu^*(\omega;W)$ with respect to W:

$$\mu^*(\omega)=\int_0^\infty n^2We^{-nW}\mu^*(\omega;W)dW$$
$$=1+(n/r)-(n/r)^2\beta(n/2r)\ , \quad \text{(B5)}$$

where n is the average density of the barriers, and the beta function is defined as

$$\beta(x)\equiv\tfrac{1}{2}[\psi(\tfrac{1}{2}(x+1))-\psi(\tfrac{1}{2}x)]$$

with $\psi(x)\equiv d\ln\Gamma(x)/dx$.

[1] J. D. Ferry, *Viscoelastic Properties of Polymers*, 3rd ed. (Wiley, New York, 1980).

[2] *Structure and Mobility in Molecular and Atomic Glasses*, edited by J. M. O'Reilly and M. Goldstein, Annals of the New York Academy of Sciences Vol. 371 (New York Academy of Sciences, New York, 1981).

[3] S. Brawer, *Relaxation in Viscous Liquids and Glasses: Review of Phenomenology, Molecular Dynamics Simulations, and Theoretical Treatment* (American Ceramic Society, Columbus, 1985).

[4] S. Matsuoka, *Relaxation Phenomena in Polymers* (Hanser, Munich, 1992).

[5] T. G Fox and P. J. Flory, J. Appl. Phys. **21**, 581 (1950); J. Phys. Chem. **55**, 221 (1951).
[6] J. Gibbs, J. Chem. Phys. **25**, 185 (1956); J. Gibbs and E. DiMarzio, *ibid.* **28**, 373 (1958); **28**, 807 (1958).
[7] M. H. Cohen and D. Turnbull, J. Chem. Phys. **31**, 1164 (1959); D. Turnbull and M. H. Cohen, *ibid.* **34**, 120 (1970).
[8] S. F. Edwards and K. E. Evans, J. Chem. Soc. Faraday Trans. 2 **78**, 113 (1982).
[9] S. F. Edwards and T. A. Vilgis, Phys. Scr. **T13**, 7 (1986).
[10] I. Teraoka and F. E. Karasz, Phys. Rev. A **45**, 5426 (1992).
[11] J. Klein, Macromolecules **11**, 852 (1978).
[12] M. Daoud and P. G. de Gennes, J. Polym. Sci. Polym. Phys. Ed. **17**, 1971 (1979).
[13] M. Doi and S. F. Edwards, J. Chem. Soc. Faraday Trans. 2 **74**, 560 (1978).
[14] P. Taborek, R. N. Kleiman, and D. J. Bishop, Phys. Rev. B **34**, 1835 (1986).
[15] M. L. Williams, R. F. Landel, and J. P. Ferry, J. Am. Chem. Soc. **77**, 3701 (1955).
[16] I. Teraoka, N. Ookubo, and R. Hayakawa, Phys. Rev. Lett. **55**, 2712 (1985).
[17] I. Teraoka and R. Hayakawa, J. Chem. Phys. **89**, 6989 (1988).
[18] When the barriers are scattered randomly in one dimension, the width W of a section between two neighboring barriers is distributed with an exponential distribution $n\exp(-nW)$, where n is the average number density of the barriers. However, the width of a section that includes the particle is distributed with $n^2W\exp(-nW)$, because a section with a larger width has a better probability of including the particle within it.
[19] S. Havriliak and S. Negami, J. Polym. Sci. Polym. Symp. **14**, 99 (1966).
[20] S. Onogi, T. Masuda, and K. Kitagawa, Macromolecules **3**, 109 (1970).
[21] G. Marin and W. W. Graessley, Rheol. Acta. **16**, 527 (1977).
[22] M. Doi and S. F. Edwards, *The Theory of Polymer Dynamics* (Clarendon, Oxford, 1986).
[23] D. A. Darling and A. J. F. Siegert, Ann. Math. Stat. **24**, 624 (1953).